Radiation Physics and Chemistry 233 (2025) 112739

Contents lists available at ScienceDirect

Radiation Physics and Chemistry

journal homepage: www.elsevier.com/locate/radphyschem

Comprehensive organ-specific radiation dose mapping in coronary angiography using the Alderson Rando phantom: *An experimental approach to optimize patient safety*

Duygu Tunçman Kayaokay [a], Fahrettin Fatih Kesmezacar [b], Nami Yeyin [c], Songül Çavdar Karaçam [a], Osman Günay [d], Turgut Karabağ [e], Mustafa Demir [f], Bashar Issa [g,h], H.O. Tekin [g,i], Ghada ALMisned [j,*]

[a] *Istanbul University – Cerrahpasa, Vocational School of Health Services, Radiotherapy Program, Istanbul, Türkiye*
[b] *Istanbul University – Cerrahpasa, Vocational School of Health Services, Medical Imaging Techniques, Istanbul, Türkiye*
[c] *Istanbul University – Cerrahpasa, Vocational School of Health Services, Nuclear Medicine Techniques, Istanbul, Türkiye*
[d] *Yıldız Technical University, Faculty of Electrical & Electronics, Biomedical Engineering, Istanbul, Türkiye*
[e] *University of Health Sciences, Istanbul Training and Research Hospital, Department of Internal Medicine, Division of Cardiology, Istanbul, Türkiye*
[f] *Istanbul University – Cerrahpaşa, Cerrahpasa Medicine Faculty, Nuclear Medicine Department, Istanbul, Türkiye*
[g] *Medical Diagnostic Imaging Department, College of Health Sciences, University of Sharjah, Sharjah, 27272, the United Arab Emirates*
[h] *Istinye University, Faculty of Engineering and Natural Sciences, Biomedical Engineering Department, Istanbul, 34396, Türkiye*
[i] *Istinye University, Faculty of Engineering and Natural Sciences, Computer Engineering Department, Istanbul, 34396, Türkiye*
[j] *Department of Physics, College of Science, Princess Nourah Bint Abdulrahman University, P.O. Box 84428, Riyadh, 11671, Saudi Arabia*

ARTICLE INFO

Handling Editor: Dr. Chris Chantler

Keywords:
Alderson Rando phantom
Coronary angiography
Dose measurement
Radiology
Radiation risk assessment

ABSTRACT

This study aimed to evaluate radiation dose distribution to critical organs, specifically the lungs, heart, and breasts, during coronary angiography using the Alderson Rando phantom. Thermoluminescent dosimeters (TLDs) were positioned at different anatomical sites within the Alderson Rando ® phantom to measure radiation exposure in a controlled simulation replicating clinical coronary angiography conditions. Our findings indicated significant variability in lung doses, with the highest exposure observed in middle lung regions due to direct alignment with the primary X-ray beam path. Cardiac dose measurements showed a relatively uniform distribution, with elevated exposure in the basal and atrial regions, reflecting their proximity to the central beam. In the breast tissue, a pronounced dose asymmetry was noted, with the right breast, particularly lateral and posterior regions, receiving substantially higher radiation due to its closer positioning to the X-ray source and increased scatter. According to results, there are different levels of radiation exposure across organs and anatomical regions during coronary angiography. It can be concluded that implementing targeted dose-reduction strategies, such as shielding and optimized angulation, is essential to protect sensitive organs, with personalized imaging protocols recommended to enhance patient safety and minimize cumulative radiation risks.

1. Introduction

With rapid advancements in medical technology, an increasing number of imaging devices employing ionizing radiation have been developed and implemented across various healthcare fields (Sardanelli, 2017). These devices are fundamental tools in diagnostic and interventional procedures, and they come in different brands and models tailored for diverse clinical applications (Gray et al., 2005). Among these, one of the most critical devices in cardiology that uses ionizing radiation is the fluoroscopy-based coronary angiography (CA) system (Sun and Jiang, 2006). Coronary angiography is a specialized diagnostic imaging procedure that visualizes the coronary arteries that are the vessels responsible for supplying oxygen-rich blood to the heart muscle (Noto et al., 1991). The technique is vital for identifying blockages, narrowing, or other abnormalities within the coronary arteries that may compromise cardiac function or lead to serious conditions such as myocardial infarction (Tavakol et al., 2012). Primarily used to diagnose and manage heart diseases like angina and coronary artery disease,

* Corresponding author.
E-mail address: gaalmisned@pnu.edu.sa (G. ALMisned).

https://doi.org/10.1016/j.radphyschem.2025.112739
Received 23 October 2024; Received in revised form 10 January 2025; Accepted 20 March 2025
Available online 21 March 2025
0969-806X/© 2025 Elsevier Ltd. All rights are reserved, including those for text and data mining, AI training, and similar technologies.

coronary angiography holds a central role in contemporary cardiology practices. It enables clinicians to obtain real-time, dynamic images through the continuous capture of X-rays provided by fluoroscopy. This imaging technique is particularly valuable as it allows for the catheter's real-time monitoring as it is maneuvered through the coronary arteries, providing critical insights for both diagnosis and treatment. The vast array of diagnostic and risk stratification data generated by these procedures plays a fundamental role in reducing the morbidity and mortality rates associated with coronary artery diseases by enabling targeted, precise interventions (Faria et al., 2023). The global increase in interventional radiology and interventional cardiology procedures in recent years reflects the expanding reliance on these advanced imaging techniques. However, this trend also highlights a growing concern: the radiation exposure experienced by patients and healthcare professionals, particularly those involved in high-frequency procedures (Coles et al., 2006; Aupongkaroon et al., 2022). It's well-known that ionizing radiation can damage cellular structures and, in the long term, may lead to cancer or other radiation-induced diseases. This issue is of particular concern for female patients undergoing procedures such as coronary angiography, as breast tissue has high radiosensitivity, making it more susceptible to radiation exposure, which can result in serious health problems. Therefore, accurately estimating and monitoring the radiation doses applied to critical organs, especially the breast, is vital for understanding and mitigating these risks. To address these risks, the ALARA (As Low As Reasonably Achievable) principle guides the use of ionizing radiation in medical settings, emphasizing that radiation doses should be minimized to the greatest extent possible while achieving the intended clinical benefits. This is especially relevant during coronary angiography, as CA procedures may involve prolonged exposure, particularly when multiple interventions are performed within a single session on the same patient. Procedures can extend to an hour or even longer, resulting in elevated cumulative radiation doses to both the patient and the medical staff working in close proximity to the radiation source (Hausleiter et al., 2009). On the other hand, organ dose estimation is fundamental in evaluating radiation-induced risks, especially regarding potential cancer risks due to exposure (Zewde et al., 2022). Specifically, mapping the dose distribution (Sanchez et al., 2015) applied to the breast tissue during coronary angiography procedures is crucial for a comprehensive understanding of the dose distribution and associated risks. Conventional dose measurement techniques, while widely used, typically offer limited information on detailed dose distribution across different tissue layers. In contrast, phantom-based studies, which use models that closely mimic human tissue characteristics, enable more accurate and in-depth analyses of radiation dose distribution. Phantoms, such as the Alderson Rando (Kesmezacar et al., 2024) phantom used in this study, are anthropomorphic models designed to simulate the density and composition of human tissues, allowing for precise measurement of radiation doses to critical organs and tissues (Xu and Eckerman, 2009). Within scientific literature, multiple approaches have been explored for estimating radiation doses to critical organs during procedures involving fluoroscopy (García Balcaza et al., 2024). Given that direct measurement of absorbed doses in internal organs is often impractical, researchers frequently employ computational models based on human anatomical structures. These models, combined with detailed geometric representations of organs, provide a basis for calculating radiation doses. Various studies have documented the use of mathematical phantoms, combined with Monte Carlo (MC) simulations, to estimate organ doses arising from radiation exposure (Fujii et al., 2017, 2020; Iriuchijima et al., 2018). Typically, dosimeters are positioned on the skin surface of the patient to gauge external doses, and Monte Carlo techniques are then employed to extrapolate organ doses based on these surface measurements. Considering these developments, this study seeks to map the radiation doses imparted to the breast during coronary angiography by utilizing an Alderson Rando phantom model. This phantom-based approach offers a means of obtaining detailed, representative dose measurements for tissues exposed to radiation during CA. Additionally, this research aims to extend dose assessments to other critical organs within the irradiation field, specifically the lungs and the heart, by experimentally measuring the radiation doses they receive during the procedure. These measurements would contribute valuable insights into organ dose distribution during coronary angiography, informing potential adjustments in clinical practices to enhance patient safety.

2. Materials and methods

In this study, thermoluminescent dosimeters (TLDs) were strategically placed on the Alderson Rando phantom to measure radiation doses received by the heart, breast, and lungs during a coronary angiography procedure. The fluoroscopy imaging was conducted based on parameters representative of an average coronary angiography performed in clinical practice (Mitsis et al., 2024). The imaging parameters used reflect the standard procedure routinely performed by a cardiologist, capturing an accurate simulation of typical exposure settings during a clinical coronary angiography session. These parameters were carefully selected to replicate real-world clinical scenarios, ensuring that the measured doses closely align with actual patient exposures under standard clinical conditions.

2.1. Alderson rando phantom

To simulate patient anatomy and tissue response in this study, the tissue-equivalent Alderson Rando phantom was utilized (see Fig. 1). The anthropomorphic Alderson Rando Phantom is a critical tool in medical imaging and radiology, designed to closely replicate human tissue interactions with ionizing radiation. Its tissue-equivalent material composition allows it to respond to radiation in a manner like actual



Fig. 1. Anthropomorphic Phantom used in Coronary Angiography Irradiation.

human tissues, making it ideal for accurate and reliable testing of radiological imaging techniques (Gandhi et al., 2015). The Alderson Rando phantom is constructed in multiple removable, interlocking sections, enabling detailed dose measurements across different anatomical regions. Each section can be easily disassembled and reassembled, allowing for precise placement of the TLDs within specific organ or tissue areas. This modularity is especially advantageous for targeted dosimetric studies, as it facilitates the measurement of radiation doses at precise depths and locations, mimicking realistic patient scenarios. In this study, TLDs were strategically positioned within the phantom to measure radiation doses in the breast, heart, and lung regions.

2.2. MTS-100 TLD dosimeters

In this study, ***MTS-100*** thermoluminescent dosimeters (TLD-100) were employed to measure radiation doses. The calibration of the TLD-100 dosimeters and subsequent dose readings following coronary angiography imaging were conducted at the Secondary Standard Dosimetry Laboratory (SSDL) of the Turkish Energy, Nuclear, and Mineral Research Agency. Dose readings from the TLDs were processed using a ***Harshaw 4500 TLD*** reader, interfaced with a computer and operated through WinREMS software. For the calibration of the dosimeter reading system, a Cesium-137 (^{137}Cs) source was used, along with an X-ray system (***Yxlon International MGC 41***) to validate the accuracy of dose readings. Reference standard dosimeters were employed as benchmarks for radiation dose measurements, allowing the calibration setup to establish a high level of accuracy and consistency in the dose data recorded for this study. It's worth mentioning that the calibration process is essential for ensuring that the TLD-100 dosimeters deliver precise and repeatable measurements, thus supporting the reliability of the radiation dose assessment performed on the Alderson Rando phantom.

2.3. Placement of dosimeters on the rando phantom

A total of 68 TLDs were carefully positioned on the Alderson Rando phantom to measure radiation doses at critical anatomical sites. Specifically, eight TLDs were placed within the lung region, eight within the heart region (see Table 1), while 32 TLDs were positioned on the anterior surface of the breasts, and 20 TLDs were placed on the posterior surface of the breasts (see Tables 2 and 3). Figs. 2 and 3 provide a schematic illustration of the TLD placements on the anterior and posterior surfaces of the right and left breasts, offering a visual guide to the dosimeter locations and their spatial distribution. In Fig. 2, the anterior views of the right breast (**A**) and left breast (**B**) display a systematic arrangement of TLDs, spaced at 4 cm intervals. This distribution includes placements both medially and laterally from the nipple (papilla mamaria), as well as above and below it. Each nipple is equipped with a pair of TLDs, marked to capture central dose data directly from the nipple area, which is a critical site for dose accumulation. The anterior surface of each breast includes 16 TLDs (i.e., eight pairs), with positioning aligned to achieve consistent measurement intervals across both breasts. The configuration was implemented in terms of accurate mapping of the dose distribution over the anterior surface, covering areas that are frequently exposed during coronary angiography. Table 2 shows the specific localization of TLDs, noting their distances from key anatomical points (e.g., 4 cm medial, 4 cm lateral, 4 cm above, and 4 cm below the nipple), facilitating a replicable layout for future studies. In Fig. 3, the posterior views of the breasts illustrate the TLD placements on the back surfaces of the right breast (**B**) and left breast (**A**). The posterior surface of each breast contains 10 TLDs (i.e., five pairs), distributed similarly to the anterior layout with precise 4 cm intervals from the nipple as a central reference.

Table 1
The placement of TLDs on the heart and lungs in the Alderson Rando phantom.

TLD No	Phantom Slice No	Localization
1–2	11	The apex of the right lung
3–4	11	The apex of the left lung
5–7	15	The middle of the right lung
8–9	15	The middle of the left lung
10–11	20	Right atrium
12–13	19	Basal of the heart
15–16	19	Left atrium
17–18	20	Apex of the heart

Table 2
Description of the localization of TLDs on the anterior surface of the Breast.

TLD No	Localization
19–20	Right papilla mamaria
26–27	4 cm medial from the right papilla mamaria
35–36	6 cm medial from the right papilla mamaria
28–29	4 cm lateral from the right areola.
33–34	8 cm lateral from the right areola.
22–23	4 cm above the right papilla mamaria
30–31	8 cm above the right papilla mamaria
24–25	4 cm below the right papilla mamaria
50–51	Left papilla mamaria
59–60	4 cm lateral from the left papilla mamaria
63–64	8 cm lateral from the left papilla mamaria
57–58	4 cm medial from the left papilla mamaria
65–66	6 cm medial from the left papilla mamaria
52–54	4 cm above the left papilla mamaria
61–62	8 cm above the left papilla mamaria
55–56	4 cm below the left papilla mamaria

Table 3
Description of the localization of TLDs on the posterior surface of the Breast.

TLD No.	Localization
37–38	Right papilla mamaria
40–41	4 cm medial from the right papilla mamaria
43–44	4 cm lateral from the right papilla mamaria
48–49	4 cm above the right papilla mamaria
46–47	4 cm below the right papilla mamaria
67–69	Left papilla mamaria
70–71	4 cm medial from the left papilla mamaria
77–78	4 cm lateral from the left papilla mamaria
75–76	4 cm below the left papilla mamaria
73–74	4 cm above the left papilla mamaria

2.4. X-ray equipment and imaging protocol

For the coronary angiography simulation, the Alderson Rando phantom was imaged using a ***Siemens Artis Zee*** coronary angiography system (***Erlangen, Germany***). This system consists of an X-ray emitter located below the patient table and an image intensifier unit positioned above. The image intensifier is equipped with an anti-scatter grid and offers three magnification modes (i.e., 30 cm, 22 cm, and 17 cm) enabling optimized visualization based on the clinical requirements. The source-to-image intensifier distances were set at 85 cm for anteroposterior (AP) views and 100 cm for oblique views, providing a clinically relevant geometry for coronary angiography imaging. Additionally, the source-to-patient distance was maintained between 70 and 80 cm on average, reflecting standard positioning in clinical procedures. The imaging protocol utilized a pulse rate of 15 pulses per second for fluoroscopy, providing low-resolution real-time imaging, and a frame rate of 7.5 frames per second for cine angiography, which captures high-resolution images. To ensure appropriate filtration and limit patient exposure, the X-ray tube was equipped with a total filtration equivalent to 4 mm of aluminum for both fluoroscopy and cine angiography modes (see Fig. 4). To define the exposure time during active imaging, patient records were examined, focusing on individuals

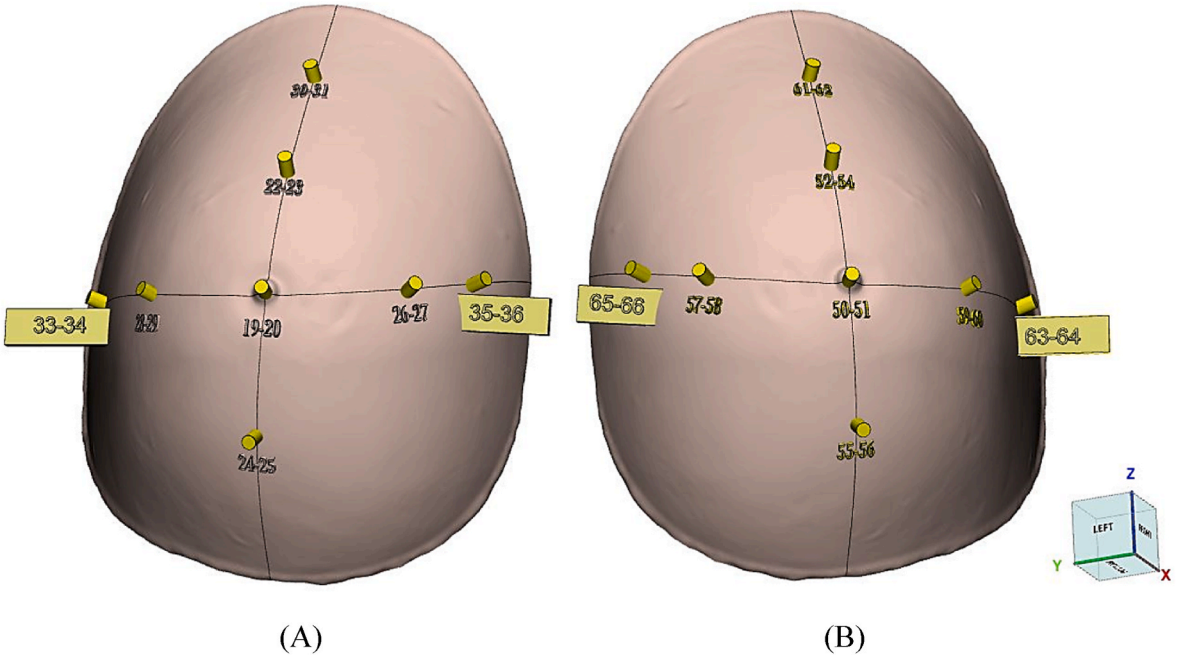


Fig. 2. Schematic of TLD placement on the breasts of the Alderson Rando phantom (anterior view). Right breast (A), left breast (B).

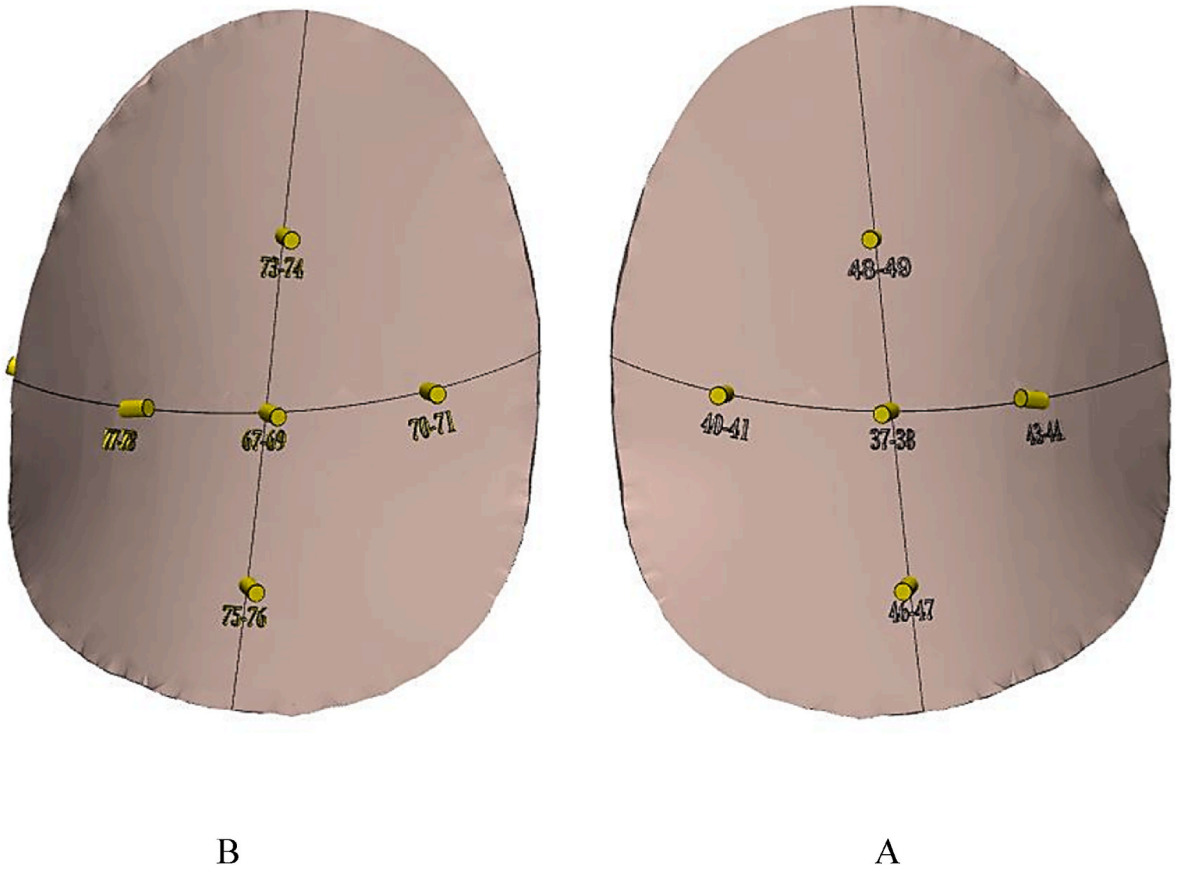


Fig. 3. Schematic of TLD placement on the breasts of the Alderson Rando phantom (posterior view). Right breast (B), left breast (A).

whose body weights were like that of the Alderson Rando phantom, approximately 55 kg. Fifteen patients were selected, each weighing between 51 and 58 kg (average 55.6 ± 3.2 kg), to simulate a realistic exposure scenario. Their average procedure durations were calculated to create a representative imaging protocol. In a standard catheterization unit, a 6 French (F) catheter is introduced via the femoral approach using the Seldinger Technique (Yuminaga et al., 2017) with fluoroscopic guidance used to monitor catheter placement in the femoral region. It's well-known that fluoroscopy provides continuous real-time X-ray imaging, allowing visualization of the coronary arteries in a

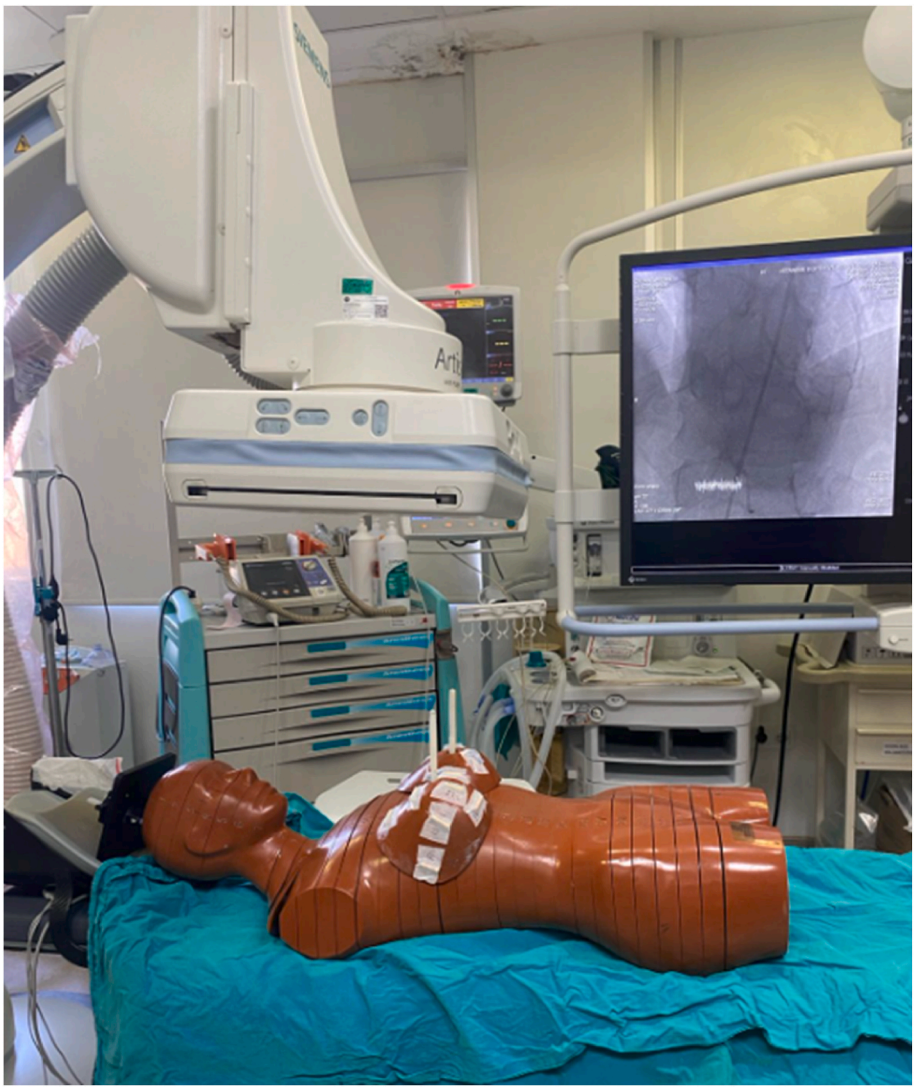


Fig. 4. Coronary Angiography Imaging of the Alderson Rando phantom set-up.

two-dimensional plane. Although image quality can be adjusted by varying the pulse rate and radiation dose, the phantom imaging was performed at 15 pulses per second, as this setting provided sufficient image quality while maintaining a clinically realistic dose. Following fluoroscopic positioning, cine angiography recordings were obtained once the catheter was positioned within the main coronary artery. Although clinical procedures like catheter insertion and manipulation were not performed on the phantom, a similar imaging protocol was

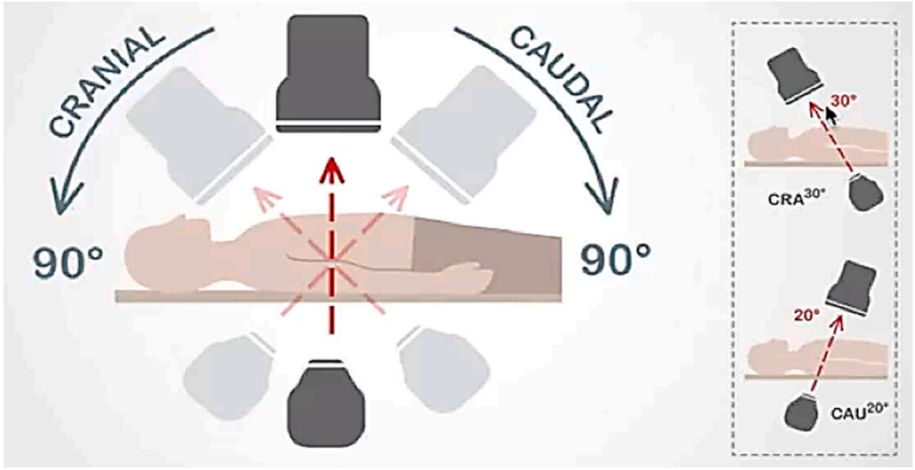


Fig. 5. Rotations applied during imaging of the Rando phantom.

maintained to ensure consistency. Prior to each cine angiography capture, brief fluoroscopy runs (5–10 s each) were used to confirm optimal positioning for each projection. The imaging projections used in this study included various standard coronary angiography views to replicate clinical imaging angles. These projections were selected to cover a range of angles that typically optimize visualization of the left coronary artery system. The following projections were used, as illustrated in Fig. 5.

- Left Anterior Oblique Caudal (LAO caudal; 35°–25°)
- Left Anterior Oblique Cranial (LAO cranial; 35°–25°)
- Anteroposterior Cranial (AP cranial; 0°–35°)
- Right Anterior Oblique Cranial (RAO cranial; 30°–25°)
- Right Anterior Oblique Caudal (RAO caudal; 35°–25°)
- Anteroposterior Caudal (AP caudal; 0°–25°)

Each projection was captured using digital cine angiography, with dedicated imaging runs recorded for each angle. Here, the aim was to enable a detailed assessment of dose distribution across different angles, simulating a complete left coronary artery evaluation, and ensuring that the radiation dose delivered to the phantom closely mirrors real-world coronary angiography procedures.

3. Results and discussion

3.1. Dose assessment for lung

The lung doses measured at various locations within the Alderson Rando phantom show considerable variation, as illustrated in Table 4. Thermoluminescent dosimeters (TLDs) were positioned at specific anatomical sites in both the right and left lungs, capturing dose differences that may result from anatomical positioning and radiation beam angles used during coronary angiography procedures, and the ensuing backscatter. The recorded doses range from a low of 1.32 mSv at TLD 1–2 (located at the apex of the right lung) to a high of 8.50 mSv at TLD 5–7 (located at the middle of the right lung). This considerable variation in dose distribution is notable, with an overall mean lung dose of 4.32 ± 3.54 mSv. The high standard deviation indicates significant dose disparity across different lung regions, which is likely influenced by the geometry of the X-ray beam and its interaction with lung tissue (Willer et al., 2018), as well as by the anatomical position of each TLD. The lower doses recorded at the lung apexes (1.32 mSv for the right apex and 1.44 mSv for the left apex) suggest that these regions receive less exposure during coronary angiography imaging. This can be attributed to the angulation of the X-ray beams (Hausmann et al., 1989), which are typically directed towards the heart and lower lung regions to maximize visualization of the coronary arteries. Conversely, the higher doses observed in the middle regions of the lungs, particularly at TLD 5–7 (8.50 mSv) and TLD 8–9 (6.02 mSv), indicate that these areas are more exposed due to their proximity to the primary beam path during oblique and anteroposterior views. These middle regions may also receive secondary scattered radiation, further contributing to the dose. Given the varying angles used in coronary angiography (Di Mario and Sutaria, 2005) (e.g., left anterior oblique, right anterior oblique, caudal, cranial), the dose distribution within the lungs is uneven. These angles are chosen to optimize coronary artery imaging but inadvertently expose the middle lung sections to higher radiation doses, as the X-ray beam traverses these regions. The positioning of the TLDs within specific lung regions (see Table 1) provides insights into how different anatomical sites within the lungs are variably exposed based on their spatial orientation relative to the X-ray source and image intensifier. The apex regions are situated further from the direct beam path, thus receiving lower doses compared to the middle lung sections. Furthermore, a closer look at this variation is justified by the fact that lower dose is expected at the apex of both sides where surrounding tissue is less than the middle of the lungs. Symmetry in shape of the apex and surrounding tissue of both sides is reflected in similar dose values across the two halves. However, dose values in TLD groups #5–7 and #8–9, which are located in the middle of the lung, are much higher than in the apex region and asymmetric in the left/right directions. The higher dose value of the right side can be justified if we consider the larger volume and higher density of lung tissues exhibited by the right side over the left side. Both factors will increase absorbed dose through scattering. The mean dose of 4.32 ± 3.54 mSv across the lung regions suggests a potential risk for radiation-induced effects in the lungs, especially with repeated coronary angiography procedures. Although the effective dose for a single procedure is within acceptable limits, cumulative exposure for patients undergoing multiple imaging sessions may increase the risk of radiation-induced pneumonitis or lung tissue damage. The high doses observed in the middle lung regions could be clinically relevant, particularly for patients with pre-existing lung conditions such as chronic obstructive pulmonary disease (COPD) or pulmonary fibrosis. These patients may be more vulnerable to the effects of radiation, necessitating careful dose optimization and monitoring. To minimize lung exposure, adjustments in the angulation and duration of each projection could be considered, particularly for patients requiring frequent imaging. Incorporating dose-saving techniques, such as reducing pulse rates and optimizing collimation, may help decrease the dose received by the middle lung regions. The observed dose disparities also highlight the importance of protective measures, such as positioning lead shields or using lower-dose settings when imaging is focused on coronary arteries rather than lung tissues. Clearly, the dose assessment for the lungs reveals significant variability in radiation exposure within different regions, reflecting the complex interplay of anatomical positioning and X-ray beam angulation during coronary angiography. Meanwhile, a statistical analysis was conducted to evaluate the significance of dose variations across the lungs, heart, and breasts. Using one-way ANOVA, the results demonstrated that the dose differences among these organs were statistically significant ($p < 0.05$). The lungs exhibited the highest dose variability, with a mean dose of 4.32 ± 3.54 mSv, largely influenced by middle lung regions (8.50 mSv). Similarly, the right breast showed considerable variability on both anterior (2.14 ± 2.6 mSv) and posterior surfaces (3.98 ± 1.44 mSv), reflecting the impact of beam angulation and scatter radiation. In contrast, the heart doses were more uniform (6.36 ± 1.29 mSv), likely due to its central position relative to the X-ray beam. These findings underscore the need for tailored imaging protocols to address organ-specific dose variability and minimize radiation risks, particularly in sensitive tissues like the lungs and breasts.

Table 4
Lung doses measured from different locations with TLDs.

TLD Number	Doses (mSv)
1–2	1.32
3–4	1.44
5–7	8.50
8–9	6.02
Mean ± SD	4.32 ± 3.54

3.2. Dose assessment for hearth

Next, we measured the cardiac doses at various anatomical locations within the Alderson Rando phantom that are relatively consistent distribution across the heart regions, as shown in Table 5. The thermoluminescent dosimeters (TLDs) were placed in different parts of the heart, including the right atrium, left atrium, basal, and apex regions, respectively. The measured doses ranged from a minimum of 5.18 mSv to a maximum of 7.86 mSv, with an overall mean cardiac dose of 6.36 ± 1.29 mSv. One can say that the relatively low standard deviation indicates a more uniform exposure pattern across the heart compared to

Table 5
Heart doses measured from different locations with TLDs.

TLD Number	Doses (mSv)
10–11	5,40
12–13	7,86
15–16	7,03
17–18	5,18
Mean ± SD	6,36 ± 1,29

the lung regions. It should be noted that the TLDs spacing is smaller in the heart than the breast or lungs (due to the organ size) which would naturally reduce dose variation. Clearly, the highest dose was recorded at TLD 12–13, located in the basal region of the heart (7.86 mSv), followed closely by TLD 15–16 in the left atrium (7.03 mSv). These elevated doses in the basal and left atrial areas can be attributed to the proximity of these regions to the central X-ray beam path, especially during left anterior oblique and anteroposterior projections commonly used in coronary angiography. Meanwhile, the lowest dose was measured at TLD 17–18, situated at the apex of the heart (5.18 mSv). The apex is anatomically positioned farther from the X-ray focal point, receiving lower exposure due to its relative distance from the primary beam, particularly in cranial and caudal views that favor imaging of the upper heart structures. The arrangement of TLDs across the heart's chambers and regions provides valuable insights into dose variation based on anatomical location. Regions closer to the X-ray source, such as the basal and atrial sections, generally received higher doses due to their alignment with common angiographic beam angles. The right atrium (TLD 10–11) exhibited a moderate dose of 5.40 mSv. This region lies somewhat peripheral to the primary imaging area in typical coronary angiographic views, resulting in slightly reduced radiation exposure compared to central cardiac structures. The mean cardiac dose of 6.36 ± 1.29 mSv, though within acceptable limits for a single procedure, raises considerations for cumulative exposure in patients undergoing repeated coronary angiography. To put it more clearly, chronic exposure could increase the risk of radiation-induced cardiac complications, such as coronary artery damage or myocardial cell injury, which are significant given the heart's sensitivity to ionizing radiation. Particularly vulnerable patient groups, such as those with pre-existing cardiac conditions, may experience heightened risk if exposed to repeated radiation doses at the levels recorded in this study. The observed dose concentration in the basal and atrial regions could have clinical relevance, as these areas are involved in vital cardiac functions, including the coordination of electrical impulses and blood flow regulation.

3.3. Dose assessment for the breasts

The breast dose measurements obtained from the Alderson Rando phantom show significant insights (Abadi et al., 2011; Foley et al., 2011; Mong et al., 2016; Sağsöz and Pirimoğlu, 2016) into the distribution of radiation across various anatomical regions within both the right and left breasts. The analysis considers both anterior (front) and posterior (back) surfaces, allowing for a detailed assessment of dose distribution within the tissue. These findings, presented in Table 6, are essential for understanding potential radiation risks associated with coronary angiography, particularly given the sensitivity of breast tissue to ionizing radiation. The mean dose on the front surface of the right breast was 2.14 ± 2.6 mSv, with individual doses ranging from 0.61 mSv (TLD 19–20, right papilla) to 8.35 mSv (TLD 33–34, 8 cm lateral from the right areola). In contrast, the left breast's front surface received a mean dose of 1.77 ± 0.79 mSv, with a range from 0.86 mSv (TLD 50–51, left papilla) to 3.1 mSv (TLD 61–62, 8 cm above the left papilla). This notable difference between the right and left breasts may be attributed to variations in positioning and angulation of the X-ray beam during coronary angiography, as the right breast tends to receive slightly higher

Table 6
Breast doses measured from different locations with TLDs.

TLD Localization	TLD Number	Dose (mSv)
Right Breast (Front)	19–20	0.61
	26–27	0.82
	35–36	1.5
	28–29	1.18
	33–34	8.35
	22–23	0.93
	30–31	2.85
	24–25	0.9
	Mean ± SD	2.14 ± 2.6
Left Breast (Front)	50–51	0.86
	59–60	1.66
	63–64	2.62
	57–58	1.6
	65–66	2.14
	52–54	1.25
	61–62	3.1
	55–56	0.94
	Mean ± SD	1.77 ± 0.79
Right Breast (Back)	37–38	4.23
	40–41	2.23
	43–44	5.87
	48–49	2.9
	46–47	4.7
	Mean ± SD	3.98 ± 1.44
Left Breast (Back)	67–69	2.34
	70–71	2.41
	77–78	3.55
	75–76	2.12
	73–74	1.5
	Mean ± SD	2.38 ± 0.74

doses due to its relative proximity to the central beam path in standard left coronary views. This is because coronary angiography procedures commonly involve a variety of angled projections (e.g., cranial and caudal views) to optimize visualization of coronary vessels (Popov et al., 2024). The angulation of these beams can inadvertently expose one breast more than the other. For instance, caudal views often involve an upward angulation of the beam, which can result in higher doses to the right breast's posterior and lateral regions, as these areas are more exposed to the deflected rays. On the other hand, the significant variation in dose values on the right breast, with a high standard deviation of 2.6 mSv, suggests that certain regions (e.g., lateral areas) are more exposed due to beam scatter and proximity to the imaging focal point. The posterior (back) surface of the right breast recorded a higher mean dose of 3.98 ± 1.44 mSv compared to the left breast's posterior mean dose of 2.38 ± 0.74 mSv. Notably, the right breast's back surface received maximum exposure at TLD 43–44 (5.87 mSv, 4 cm lateral from the right papilla), likely due to the increased scatter radiation in this region. The left breast's back surface doses were generally lower, with a maximum of 3.55 mSv (TLD 77–78, 4 cm lateral from the left papilla). The dose distribution along the front/back direction shows larger dose (mean across left and right sides) for the back 3.18 mSv than the front 1.96 mSv. This is expected as the back side represents the entrance dose and also there is more possibility of back scatter for the back side than the front side. For the left/right sides, lower mean value (averaged over front and back sides) of 2.08 mSv is observed for the left than the right side of 3.06 mSv. This can be explained by the fact that the position of the heart on the left side can be acting as a stronger attenuator than lung tissue [Ref: mu for hears vs lung]. Instead of looking at the standard variation (SD) over the four values (left/right or L/R and front/back or F/B), we used the coefficient of variation (CoV) or the relative standard deviation (RSD). All values (in mSv) were close to each other, Left/Front (LF) side 0.45, LB side 0.31, RB side 0.36, except for RF side 1.21. This could be attributed to the angulation of the beam and the absence of scattering. The reduced exposure on the left breast's posterior surface could reflect positioning factors that shield this side from higher-intensity scatter (such as heart), indicating that anatomical

placement relative to the X-ray beam significantly impacts dose distribution. The regions situated laterally on both the anterior and posterior surfaces of the breasts exhibit consistently higher dose values, particularly on the right breast (e.g., TLD 33–34 and TLD 43–44). These lateral regions are more susceptible to scatter radiation, as they are closer to the beam path during common left-oblique and anterior-posterior views used in coronary imaging. The medial areas, by contrast, received lower doses, with TLDs positioned 4–6 cm medial from the papilla on both sides showing consistently low values. This distribution pattern confirms the role of beam angle and scatter in shaping dose exposure across breast tissue. Meanwhile, the high doses observed in lateral regions, particularly on the right breast, raise concerns about localized radiation exposure in sensitive breast tissue. Given the radiosensitivity of breast tissue (Di Maria et al., 2024) and its association with increased cancer risk (John et al., 2007), these dose variations are clinically significant. Repeated exposure to high doses, especially in lateral regions, could elevate the risk of radiation-induced malignancies (Chan et al., 2017). The observed discrepancies in dose between the right and left breasts highlight a potential for asymmetric radiation exposure during coronary procedures. This asymmetry can be attributed to the varied angulations employed during coronary angiography, such as cranial, caudal, and oblique projections. These angles are designed to optimize visualization of coronary vessels but may inadvertently increase exposure to regions closer to the X-ray source. For instance, caudal views often involve an upward beam trajectory, which intensifies radiation exposure to the posterior and lateral regions of the right breast. This phenomenon underlines the critical need for dose-optimization strategies, including minimizing beam angulation in regions prone to higher scatter and implementing tailored shielding protocols. The right breast's higher average doses and greater dose variability suggest a higher cumulative risk, especially in patients undergoing multiple procedures. These findings underscore the importance of dose optimization and careful angulation to minimize unnecessary radiation exposure to sensitive breast tissue. To assess the clinical significance of the observed breast doses, we compared the measured values with established safety thresholds for radiation exposure. According to the International Commission on Radiological Protection (ICRP) guidelines, the recommended annual dose limit for the breast tissue in medical settings is 20 mSv for occupational exposures and lower for patients undergoing diagnostic procedures. The mean anterior breast dose recorded in our study (2.14 $\pm$ 2.6 mSv for the right breast, 1.77 $\pm$ 0.79 mSv for the left breast) remains well below these thresholds. However, localized regions, such as the lateral areas of the right breast, showed doses as high as 8.35 mSv, highlighting the potential for higher cumulative exposure in patients undergoing repeated procedures. These findings emphasize the need for strict adherence to dose-reduction strategies, such as optimized beam angulation and the use of protective shielding, to maintain dose levels within acceptable safety margins. The substantial standard deviation in dose measurements, particularly on the right breast's front surface (SD $=$ 2.6 mSv), suggests that certain regions are disproportionately exposed compared to others. This variability may be influenced by patient-specific anatomical differences, procedural angle adjustments, and secondary scatter radiation. The relatively lower standard deviations on the left breast (front SD $=$ 0.79 mSv, back SD $=$ 0.74 mSv) indicate a more consistent dose distribution, potentially due to shielding from direct exposure angles. This reduced dose variability on the left breast could mitigate some of the cumulative radiation risks, but the lateral regions still exhibit elevated doses that necessitate attention. It's worth mentioning that some modifications to imaging protocols could include adjusted angulation and selective shielding of lateral breast areas to minimize breast radiation exposure, especially in high-dose lateral regions. Applying lead shielding or utilizing oblique angles that avoid direct exposure to the breasts could further reduce dose accumulation in these sensitive regions. Furthermore, awareness of dose variability between breast regions could help guide personalized dose management strategies. For patients requiring frequent imaging, shielding protocols should prioritize the right breast, particularly the lateral and posterior regions, where cumulative dose exposure is more likely.

4. Conclusions

This study provides a comprehensive evaluation of radiation dose distribution to the lungs, heart, and breasts during coronary angiography using the Alderson Rando phantom. The findings showed significant variability in dose exposure, shaped by anatomical positioning, beam angles, and scatter radiation.

- Lung doses varied considerably, with higher exposure in middle regions, potentially increasing the risk of radiation-induced lung effects in patients undergoing repeated procedures, particularly those with pre-existing pulmonary conditions.
- In contrast, cardiac doses displayed a more consistent pattern, with elevated exposure in the basal and atrial regions due to proximity to the central beam path.
- While within acceptable limits, cumulative exposure from repeated angiography could elevate the risk of cardiac complications, especially for vulnerable patients.
- A key finding was the notable dose asymmetry between the right and left breasts; the right breast, particularly in lateral and posterior regions, consistently received higher exposure due to its anatomical proximity to the X-ray beam, raising concerns about cumulative radiation risk to breast tissue, known for its radiosensitivity.

This dose discrepancy shows the need for dose-reduction strategies, including shielding and protocol optimization to minimize unnecessary exposure, particularly for patients undergoing multiple angiographies. Despite its valuable insights, this study's limitations include its reliance on a phantom model, which cannot fully replicate individual anatomical differences, the use of a single imaging protocol that may not encompass procedural variations, and the absence of motion simulation, which is relevant for assessing dynamic organ dose. Moreover, the use of the Alderson Rando phantom provides controlled conditions for dose measurements, but it lacks the physiological complexity of real patients. For instance, patient-specific factors such as varying body habits, organ motion due to respiration or cardiac activity, and tissue density variations can significantly influence radiation dose distribution. Furthermore, the static nature of the phantom does not account for dynamic changes during live coronary angiography procedures, such as catheter manipulation or patient positioning adjustments. These differences may result in discrepancies when translating phantom-based dose estimations to actual clinical scenarios. Addressing these limitations in future studies through patient-based validation or the incorporation of dynamic phantom models could improve the accuracy and applicability of dose assessments in real-world settings. Therefore, future studies should validate these findings in patient-based models, investigate advanced dose reduction techniques, incorporate dynamic organ modeling, and consider longitudinal patient follow-up to better understand long-term effects. Future research could also benefit from the integration of dynamic organ models that simulate respiratory and cardiac motion during imaging. Such models would allow for more accurate assessment of dose distribution in real-time, bridging the gap between phantom-based studies and clinical applications. Additionally, exploring advanced imaging techniques, such as motion-compensated dose mapping and real-time adaptive shielding, could further enhance patient safety and reduce radiation risks during coronary angiography. It can be concluded that targeted radiation protection strategies are crucial in coronary angiography to minimize radiation exposure to critical organs such as the lungs, heart, and breasts. It can be also concluded that implementing dose-reduction techniques and optimizing clinical practices will not only enhance patient safety but also lower the long-term risks associated with repeated imaging procedures.

CRediT authorship contribution statement

Duygu Tunçman: Writing – original draft, Investigation, Formal analysis, Data curation, Conceptualization. **Fahrettin Fatih Kesmezacar:** Methodology, Investigation, Data curation. **Nami Yeyin:** Methodology, Investigation, Data curation. **Songül Çavdar Karaçam:** Methodology, Investigation, Data curation. **Osman Günay:** Formal analysis, Data curation. **Turgut Karabağ:** Investigation, Data curation. **Mustafa Demir:** Methodology, Investigation, Data curation. **Bashar Issa:** Investigation. **H.O. Tekin:** Writing – original draft, Investigation, Formal analysis, Data curation. **Ghada Almisned:** Writing – original draft, Methodology, Investigation, Data curation.

Funding

Princess Nourah bint Abdulrahman University Researchers Supporting Project number (PNURSP2025R149), Princess Nourah bint Abdulrahman University, Riyadh, Saudi Arabia.

Declaration of competing interest

The authors declare that they have no known competing financial interests or personal relationships that could have appeared to influence the work reported in this paper.

Acknowledgements

The authors would like to express their deepest gratitude to Princess Nourah bint Abdulrahman University Researchers Supporting Project number (**PNURSP2025R149**), Princess Nourah bint Abdulrahman University, Riyadh, Saudi Arabia.

Data availability

Data will be made available on request.

References

Abadi, S., Mehrez, H., Ursani, A., Parker, M., Paul, N., 2011. Direct quantification of breast dose during coronary CT angiography and evaluation of dose reduction strategies. Am. J. Roentgenol. 196 (2), W152–W158. https://doi.org/10.2214/AJR.10.4626.

Aupongkaroon, P., Makarawate, P., Chaosuwannakit, N., 2022. Comparison of radiation dose and its correlates between coronary computed tomography angiography and invasive coronary angiography in Northeastern Thailand. Egyptian Heart Journal 74 (1), 6. https://doi.org/10.1186/s43044-022-00241-5.

Chan, S., Chen, J.H., Li, S., Chang, R., Yeh, D.C., Chang, R.F., Yeh, L.R., Kwong, J., Su, M. Y., 2017. Evaluation of the association between quantitative mammographic density and breast cancer occurred in different quadrants. BMC Cancer 17 (1), 274. https://doi.org/10.1186/s12885-017-3270-0.

Coles, D.R., Smail, M.A., Negus, I.S., Wilde, P., Oberhoff, M., Karsch, K.R., Baumbach, A., 2006. Comparison of radiation doses from multislice computed tomography coronary angiography and conventional diagnostic angiography. J. Am. Coll. Cardiol. 47 (9), 1840–1845. https://doi.org/10.1016/j.jacc.2005.11.078.

Di Maria, S., van Nijnatten, T.J.A., Jeukens, C.R.L.P.N., Vedantham, S., Dietzel, M., Vaz, P., 2024. Understanding the risk of ionizing radiation in breast imaging: concepts and quantities, clinical importance, and future directions. Eur. J. Radiol. 181, 111784. https://doi.org/10.1016/j.ejrad.2024.111784.

Di Mario, C., Sutaria, N., 2005. Coronary angiography in the angioplasty era: projections with a meaning. Heart 91 (7), 968–976. https://doi.org/10.1136/hrt.2005.063107.

Faria, D., Hennessey, B., Shabbir, A., Mejía-Rentería, H., Wang, L., Lee, J.M., Matsuo, H., Biscaglia, S., Koo, B.K., Xu, B., Baptista, S., Gonzalo, N., Escaned, J., 2023. Functional coronary angiography for the assessment of the epicardial vessels and the microcirculation. EuroIntervention 19 (3), 203–221. https://doi.org/10.4244/EIJ-D-22-00969.

Foley, S.J., McEntee, M.F., Achenbach, S., Brennan, P.C., Rainford, L.S., Dodd, J.D., 2011. Breast surface radiation dose during coronary CT angiography: reduction by breast displacement and lead shielding. Am. J. Roentgenol. 197 (2), 367–373. https://doi.org/10.2214/ajr.10.4569.

Fujii, K., Nomura, K., Muramatsu, Y., Obara, S., Akahane, K., Kusumoto, M., 2017. Organ dose evaluations based on Monte Carlo simulation for CT examinations using tube current modulation. Radiat. Protect. Dosim. 174 (3), 387–394. https://doi.org/10.1093/rpd/ncw144.

Fujii, K., Nomura, K., Muramatsu, Y., Goto, T., Obara, S., Ota, H., Tsukagoshi, S., 2020. Correlation analysis of organ doses determined by Monte Carlo simulation with dose metrics for patients undergoing chest-abdomen-pelvis CT examinations. Phys. Med. 77, 1–9. https://doi.org/10.1016/j.ejmp.2020.07.016.

Gandhi, D., Crotty, D.J., Stevens, G.M., Schmidt, T.G., 2015. Technical note: phantom study to evaluate the dose and image quality effects of a computed tomography organ-based tube current modulation technique. Med. Phys. 42 (11), 6572–6578. https://doi.org/10.1118/1.4933197.

García Balcaza, V., Barceló Pagès, M., Ruiz Martínez, A., Camp, A., Ginjaume, M., Duch, M.A., 2024. Comparison of experimental measurements and fast Monte Carlo simulations for typical set-ups in fluoroscopically-guided interventional procedures. Radiat. Meas. 175, 107146. https://doi.org/10.1016/j.radmeas.2024.107146.

Gray, J.E., Archer, B.R., Butler, P.F., Hobbs, B.B., Mettler Jr., F.A., Pizzutiello Jr., R.J., Schueler, B.A., Strauss, K.J., Suleiman, O.H., Yaffe, M.J., 2005. Reference values for diagnostic radiology: application and impact. Radiology 235 (2), 354–358. https://doi.org/10.1148/radiol.2352020016.

Hausleiter, J., Meyer, T., Hermann, F., Hadamitzky, M., Krebs, M., Gerber, T.C., McCollough, C., Martinoff, S., Kastrati, A., Schömig, A., Achenbach, S., 2009. Estimated radiation dose associated with cardiac CT angiography. JAMA 301 (5), 500–507. https://doi.org/10.1001/jama.2009.54.

Hausmann, E., Allen, K., Christersson, L., Genco, R.J., 1989. Effect of x-ray beam vertical angulation on radiographic alveolar crest level measurement. J. Periodontal. Res. 24 (1), 8–19. https://doi.org/10.1111/j.1600-0765.1989.tb00852.x.

Iriuchijima, A., Fukushima, Y., Ogura, A., 2018. Comparison of organ dose calculation using Monte Carlo simulation and in-phantom dosimetry in CT examination. Nippon. Hoshasen Gijutsu Gakkai Zasshi 74 (2), 166–171. https://doi.org/10.6009/jjrt.2018_JSRT_74.2.166 (in Japanese).

John, E.M., Phipps, A.I., Knight, J.A., Milne, R.L., Dite, G.S., Hopper, J.L., Andrulis, I.L., Southey, M., Giles, G.G., West, D.W., Whittemore, A.S., 2007. Medical radiation exposure and breast cancer risk: findings from the Breast Cancer Family Registry. Int. J. Cancer 121 (2), 386–394. https://doi.org/10.1002/ijc.22668.

Kesmezacar, F.F., Tunçman, D., Nayci, A.E., Günay, O., Yeyin, N., Üzüm, G., Demir, M., Akkuş, B., Elshami, W., Almisned, G., Tekin, H.O., 2024. In-depth exploration of the radiation exposure to staff performing endoscopic retrograde cholangiopancreatography procedures (ERCP) through RANDO phantom and TLDs. Jpn. J. Radiol. 42 (9), 1058–1066. https://doi.org/10.1007/s11604-024-01586-4.

Mitsis, A., Eftychiou, C., Kadoglou, N.P.E., Theodoropoulos, K.C., Karagiannidis, E., Nasoufidou, A., Ziakas, A., Tzikas, S., Kassimis, G., 2024. Innovations in intracoronary imaging: present clinical practices and future outlooks. J. Clin. Med. 13 (14), 4086. https://doi.org/10.3390/jcm13144086.

Mong, K.S., Wallace, A.B., Franich, R.D., 2016. Asymmetric breast dose in coronary angiography. J. Appl. Clin. Med. Phys. 17 (2), 532–541. https://doi.org/10.1120/jacmp.v17i2.5746.

Noto Jr., T.J., Johnson, L.W., Krone, R., Weaver, W.F., Clark, D.A., Kramer Jr., J.R., Vetrovec, G.W., 1991. Cardiac catheterization 1990: a report of the registry of the society for cardiac angiography and interventions (SCA&I). Catheter. Cardiovasc. Diagn. 24 (2), 75–83. https://doi.org/10.1002/ccd.1810240202.

Popov, M., Amanturdieva, A., Zhaksylyk, N., Alkanov, A., Saniyazbekov, A., Aimyshev, T., Ismailov, E., Bulegenov, A., Kuzhukeyev, A., Kulanbayeva, A., Kalzhanov, A., Temenov, N., Kolesnikov, A., Sakhov, O., Fazli, S., 2024. Dataset for automatic region-based coronary artery disease diagnostics using X-ray angiography images. Sci. Data 11 (1), 20. https://doi.org/10.1038/s41597-023-02871-z.

Sağsöz, M.E., Pirimoğlu, R.B., 2016. Radiation dose to breasts from a cardiac computed tomography angiography scanogram can be reduced by switching tube position. Turk. J. Med. Sci. 46 (5), 1306–1308. https://doi.org/10.3906/sag-1408-49.

Sanchez, R.M., Vano, E., Fernandez, J.M., Escaned, J., 2015. Evaluation of a real-time display for skin dose map in cardiac catheterisation procedures. Radiat. Protect. Dosim. 165 (1–4), 240–243. https://doi.org/10.1093/rpd/ncv033.

Sardanelli, F., 2017. Trends in radiology and experimental research. European Radiology Experimental 1, 1. https://doi.org/10.1186/s41747-017-0006-5.

Sun, Z., Jiang, W., 2006. Diagnostic value of multislice computed tomography angiography in coronary artery disease: a meta-analysis. Eur. J. Radiol. 60 (2), 279–286. https://doi.org/10.1016/j.ejrad.2006.06.009.

Tavakol, M., Ashraf, S., Brener, S.J., 2012. Risks and complications of coronary angiography: a comprehensive review. Global J. Health Sci. 4 (1), 65–93. https://doi.org/10.5539/gjhs.v4n1p65.

Willer, K., Fingerle, A.A., Gromann, L.B., De Marco, F., Herzen, J., Achterhold, K., Gleich, B., Muenzel, D., Scherer, K., Renz, M., Renger, B., Kopp, F., Kriner, F., Fischer, F., Braun, C., Auweter, S., Hellbach, K., Reiser, M.F., Schroeter, T., Mohr, J., Yaroshenko, A., Maack, H.I., Pralow, T., van der Heijden, H., Proksa, R., Koehler, T., Wieberneit, N., Rindt, K., Rummeny, E.J., Pfeiffer, F., Noël, P.B., 2018. X-ray dark-field imaging of the human lung – a feasibility study on a deceased body. PLoS One 13 (9), e0204565. https://doi.org/10.1371/journal.pone.0204565.

Xu, X.G., Eckerman, K.F. (Eds.), 2009. Handbook of Anatomical Models for Radiation Dosimetry, first ed. CRC Press. https://doi.org/10.1201/EBK1420059793.

Yuminaga, Y., Kam, J., Louie-Johnsun, M., 2017. Multi-centre, prospective evaluation of the Seldinger technique for difficult male urethral catheter insertions by non-urology trained doctors. BJU Int. 120 (Suppl. 3), 21–27. https://doi.org/10.1111/bju.13928.

Zewde, N., Ria, F., Rehani, M.M., 2022. Organ doses and cancer risk assessment in patients exposed to high doses from recurrent CT exams. Eur. J. Radiol. 149, 110224. https://doi.org/10.1016/j.ejrad.2022.110224.